ELSEVIER

Chemical Physics 196 (1995) 395–406

Chemical Physics

Spin–orbit configuration interaction study of the electronic spectrum of antimony iodide

Kalyan K. Das [1], Aleksey B. Alekseyev [2], Heinz-Peter Liebermann, Gerhard Hirsch, Robert J. Buenker

Bergische Universität – Gesamthochschule Wuppertal, Fachbereich 9 – Theoretische Chemie, Gaussstrasse 20, D-42097 Wuppertal, Germany

Received 23 March 1995

Abstract

Relativistic effective core potentials (RECPs) have been employed in the framework of a spin–orbit configuration interaction (CI) approach to compute potential energy curves for the lowest-lying electronic states of the SbI molecule, as well as the Einstein coefficients of spontaneous emission for transitions between them. In contrast to systems such as arsenic and antimony fluoride, it is found that the lowest $^3\Pi$ state of SbI is repulsive, and a qualitative explanation for this distinction in terms of the electronegativity difference of the constituent atoms is put forward. The computed T_e value of the a $^1\Delta_2$ state is in good agreement with a result inferred on the basis of experimental b 0^+ and a $^1\Delta_2$ T_e values in other group VA–VIIA and VIA–VIA systems. Two different semicore and full-core RECPs have been employed at various levels of sophistication in the spin–orbit CI treatment to obtain the present results and the corresponding findings are in generally good agreement with one another. The intensity of the b–X_1 transition is computed to be much larger than that of b–X_2, in agreement with the observations of Winter et al. The fact that the opposite relationship has been found for SbF and many other diatomics in which the halogen is the lighter of the two atoms, as first pointed out by Colin et al., is discussed and also found to be closely tied up with electronegativity considerations.

1. Introduction

The antimony iodide molecule is isovalent with oxygen and consists of two elements from the fourth row of the periodic table. Its low-energy spectrum is thus characterized by a $^3\Sigma^-$ ground state, with a fairly large zero-field splitting caused primarily by the spin–orbit interaction for such heavy atoms, followed by $^1\Delta$ and $^1\Sigma^+$ excited states which come from the same π^{*2} electronic configuration. Winter et al. [1] have studied the b $^1\Sigma^+$–X_1 0^+ and b $^1\Sigma^+$–X_2 1 transitions in chemiluminescence experiments in the near infrared. These authors have found a large disparity in the intensities of these two band systems, with that of b–X_2 only 1.3% as strong as b–X_1 [1]. This behavior is consistent with previous

[1] Marie-Curie fellow, Commission of the European Communities.

Permanent address: Department of Chemistry, Physical Chemistry Section, Jadavpur University, Calcutta 700032, India.

[2] Fellow of the Alexander von Humboldt Foundation.

0301-0104/95/$09.50 © 1995 Elsevier Science B.V. All rights reserved
SSDI 0301-0104(95)00140-9

experience for other group VA–VIIA diatomics, as first pointed out by Colin et al. [2], which also indicates that the opposite intensity relationship occurs whenever the halogen constituent is lighter than that from the nitrogen family. Recent spin–orbit CI calculations for the SbF molecule [3], for example, found that the b–X_2 Einstein coefficient in this case is 38 times larger than that for b–X_1. In BiF the situation is complicated by the fact that the b $^1\Sigma^+$ interacts strongly with the $\pi^* \rightarrow \sigma^*$ $^3\Pi$ state because of the increased importance of spin–orbit coupling in this system [4].

The SbI molecule differs from the latter two isovalent systems in at least two important ways. First, the electronegativities of the two constituents lie much closer together than for either of the fluorides. In addition, the spin–orbit interaction is strong for electrons near both the antimony and iodine atoms, not just for the group VA species. Previous calculations [3,4] also indicate that the intensity ratio in question depends on the value of the equilibrium distance for a given system, because the key electronic dipole moments vary strongly with r, contrary to what is assumed in the Franck–Condon principle.

A second important open question in this molecule's electronic spectrum is the location of the a $^1\Delta$ state, which has not yet been observed in direct measurements [1]. Bielefeld et al. [5] have reviewed the experimental data available for a large number of isovalent systems, including O_2, S_2, SO and SeO in the group VIA–VIA diatomics and NF, NCl, NBr, NI, AsF and SbF among the group VA–VIIA members, and on this basis they have arrived at an estimate for the a–X_1 T_e value of 6780 cm^{-1}. The a $^1\Delta$ state has a dipole-allowed transition to X_2 1 in the ω–ω coupling scheme but it is spin- and dipole-forbidden according to the Λ–S selection rules and the low energy of the a–X_2 transition also tends to mitigate against the occurrence of strong transitions. It is therefore of interest to calculate this T_e value employing ab initio CI methods to obtain an independent estimate of this quantity, especially since comparison can be made with analogous calculations for molecules for which the corresponding experimental results are known. More generally, it would be helpful to have detailed information regarding the high-energy portion of the SbI spectrum, since emission from a suitable upper state down to a $^1\Delta$ may be relatively easy to observe, ultimately leading to the desired experimental determination of its T_e value.

In the last several years relativistic effective core potentials (RECPs) have been employed in conjunction with spin–orbit CI calculations to investigate the electronic spectra of related systems, including AsF [6], SbO [7] and BiO [8], in addition to SbF [3] and BiF [4,9] already mentioned. In the present application to the antimony iodide molecule, two different RECPs will be considered from LaJohn et al. [10]. The simpler (full-core) RECP includes all but the 5s and 5p shells in the potential, while the other (semicore) leaves the 4d as well as the 5s, 5p electron distribution to be described by AO basis functions. Both potential energy curves and intensities will be computed in each case in order to afford a suitably broad comparison between these two RECPs. An important aspect in the theoretical treatment is the description of the asymptotic behavior of the various molecule states of SbI. More generally comparison of the present results with analogous data from CI calculations for a large number of such group VA–VIIA diatomics should be quite useful in understanding the role of relativistic effects in determining the appearance of the electronic spectra in this series of electron-rich molecules.

2. Computational methods

Two different RECPs are compared in the present study, the semicore (ECP1) and full-core (ECP2) given by LaJohn et al. [10] for both the Sb and I atoms. The Cartesian Gaussian AO basis set chosen for the full-core calculations is the (3s3p) set from the original reference [10] employed in uncontracted form, augmented with a d function with optimized exponent (0.22 a_0^{-2} for Sb and 0.285 a_0^{-2} for I). The semicore calculations also make use of the original (3s3p4d) AO basis sets given for this RECP [10], except that a [211] contraction is used for the d primitives based on the coefficients recommended for the functions with the two largest exponents. An SCF calculation is carried out for the π^{*2} $^3\Sigma^-$ ground state for all valence electrons (32 for ECP1 and 12 for ECP2) at each internuclear distance considered (in the 4.0–9.0 a_0 range). The resulting SCF-MOs are employed as one-electron functions

for the ensuing CI treatment for a large number of electronic states. The 4d-type MOs are held doubly occupied in the semicore study, so twelve active electrons are present in all CI calculations. The comparison between the two RECPs thus centers on the question of whether there are advantages in describing the Sb and I 4d electrons with AO basis functions in a fixed core as opposed to simply including them in the effective core potentials directly, but there are other differences in the accompanying CI treatments as well.

The multireference singles and doubles CI method (MRD-CI [11]) is employed throughout for the Λ–S calculations which neglect the influence of spin–orbit coupling but include other spin-independent relativistic interactions. The Table CI algorithm [12] is used for efficient handling of the complicated open-shell relationships which arise in such calculations. A series of key reference configurations is defined for a number of low-lying electronic states of a given Λ–S symmetry from which all singly and doubly excited configurations are generated. A standard perturbative scheme [11] is employed in conjunction with the solution of secular equations for selected CI subspaces to obtain the corresponding energy eigenvalues, and the multireference analogue of the Davidson correction [13–15] is applied to obtain an accurate estimate of the corresponding full CI result in the same AO basis. All calculations are carried out in the C_{2v} subgroup, although the SCF-MOs themselves transform as irreducible representations of the full $C_{\infty v}$ linear group. Details regarding the numbers of reference configurations and roots treated for each of twelve Λ–S symmetries (singlets, triplets and quintets) are given in Table 1. Sizes of the corresponding generated and selected CI spaces are also included, as well as the $C_{\infty v}$ notation for the lowest roots and the $\sum c_p^2$ values for the reference configuration coefficients in the final ECP1 CI eigenfunctions (for $r = 5.20\ a_0$).

The Λ–S eigenfunctions are then employed as basis functions for the spin–orbit CI treatment. The resulting secular equation orders are 46×46 for the A_1, B_1 and B_2 irreducible representations of the C_{2v} double group and 47×47 for A_2 in the calculations carried out with the semicore RECP. The orders are smaller for the full-core treatment: 13×13 for A_1 and 11×11 for the other three representations. A selection threshold of $T = 10.0\ \mu E_h$ has been chosen for ECP2, while a value of $T = 5.0\ \mu E_h$ is taken in the semicore treatment.

Table 1
Technical details of the MRD-CI calculations (ECP1) for the SbI molecule at $T = 5\ \mu E_h$ [a]

C_{2v}	N_{ref}/N_{root}	SAFTOT/SAFSEL	$C_{\infty v}$	$\sum c_p^2$
$^1A_1$	140/6	2325602/9580	$^1\Delta$	0.9476
			$^1\Sigma^+$	0.9456
$^1B_{1,2}$	131/5	2664852/8993	$1\ ^1\Pi_{x,y}$	0.9425
			$2\ ^1\Pi_{x,y}$	0.9378
$^1A_2$	125/6	2603822/10618	$^1\Delta$	0.9523
			$^1\Sigma^-$	0.9391
$^3A_1$	132/6	4738340/11351	$^3\Delta$	0.9455
			$^3\Sigma^+$	0.9453
$^3B_{1,2}$	123/5	4904194/11204	$1\ ^3\Pi_{x,y}$	0.9443
			$2\ ^3\Pi_{x,y}$	0.9407
$^3A_2$	118/5	5285265/9482	$^3\Sigma^-$	0.9470
			$^3\Delta$	0.9436
$^5A_1$	134/5	5814015/9115	$^5\Delta$	0.9388
			$^5\Sigma^+$	0.9385
$^5B_{1,2}$	163/5	5353401/13983	$1\ ^5\Pi_{x,y}$	0.9450
			$2\ ^5\Pi_{x,y}$	0.9381
$^5A_2$	133/5	5344910/11547	$1\ ^5\Sigma^-$	0.9481
			$2\ ^5\Sigma^-$	0.9480

[a] The number of selected SAFs and $\sum c_p^2$ values are given for $r = 5.20\ a_0$. SAFTOT designates the total number of generated, SAFSEL the number of selected SAFs. N_{ref} and N_{root} refer to the number of reference configurations and roots treated, respectively.

The wavefunctions resulting from the diagonalizations in the selected CI spaces are taken to compute the required spin–orbit coupling integrals in the relativistic Hamiltonian matrix representation, whereas the estimated full CI energies are placed in the corresponding diagonal blocks for pairs of functions of the same Λ–S type. The selected CI wavefunctions have also been employed to calculate electric dipole matrix elements for use in the computation of Einstein coefficients of spontaneous emission. More details of the present spin–orbit CI treatment may be found elsewhere [3,8]. Vibrational calculations are then carried out by means of the Numerov–Cooley numerical method [16,17]. The resulting eigenfunctions are employed to compute vibrational transition moments. These results are combined with corresponding transition energies to compute Einstein coefficients for pairs of vibrational functions and the corresponding radiative lifetimes are computed by

summing over these quantities for all lower-lying levels and inverting [3].

3. Results of the CI calculations

3.1. Λ–S potential curves

The calculated Λ–S potential energy curves are shown in Fig. 1. The X $^3\Sigma^-$ ground state dissociates to the $Sb(^4S_u) + I(^2P_u)$ atomic limit. Three other electronic states go to the same asymptote, $^3\Pi$, $^5\Pi$ and $^5\Sigma^-$, and each of their potential curves is seen to be repulsive. Such behavior is the norm for the two quintet states in this class of molecules, but many examples of bound 1 $^3\Pi$ potential curves are known, such as for the fluorides of arsenic, antimony and bismuth [3,4,6]. The $\Omega = 0^+$ component of this $^3\Pi$ state plays a key role in spectroscopic observations of the group VA–VIIA diatomics, generally becoming the dominant Λ–S state at large r values for the

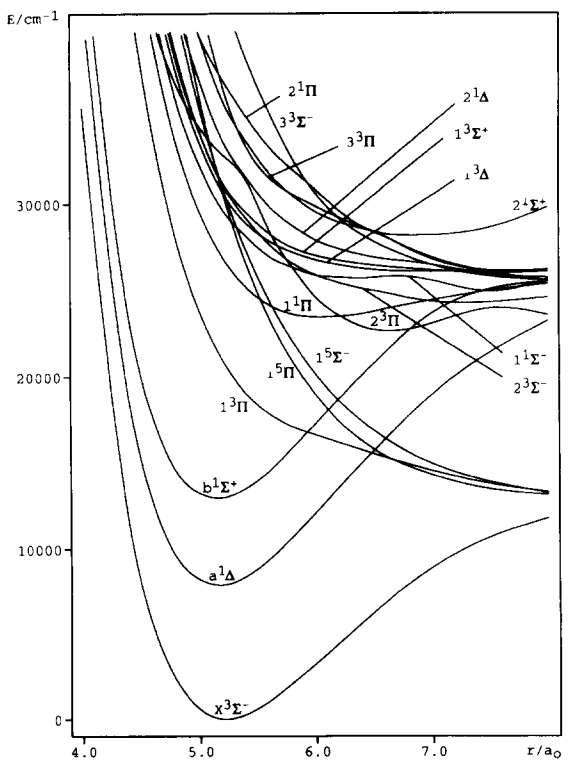

Fig. 1. Potential energy curves of the low-lying Λ–S states of SbI calculated without spin–orbit interaction.

lowest excited state of this symmetry. Thus a qualitative explanation for the contrasting appearances of the $^3\Pi$ potential curves for SbF and SbI would be most welcome.

It appears to be tied up with the different natures of the molecular orbitals in the two cases. Because fluorine is so much more electronegative than antimony, the σ and π MOs of SbF are found to be rather strongly localized. The situation is nearly opposite in SbI. As a result, the σ^* MO in SbF is far less antibonding than in the iodide system and hence its occupation in the $\ldots\sigma^2\pi^4\pi^*\sigma^*$ $^3\Pi$ state leads to only a moderate decrease in bond strength relative to X $^3\Sigma^-$ in which it is not occupied at all. There is a much stronger antibonding effect in SbI, however, which seems to be primarily responsible for the repulsive nature of its lowest $^3\Pi$ state. The localization in the π orbitals of SbF [3] and BiF [4] is well known to have an important effect on the ground state zero-field splittings of these two molecules. The π^* orbital, which is doubly occupied in the ground state, has a great deal of heavy-atom character in each case, thereby maximizing the effect of spin–orbit coupling for both systems. We will see subsequently in Section 3.3. that the degree of localization of the SCF-MOs in the group VA halides is also a key factor in understanding Colin's rules for the relative strengths of their respective b–X_1 and b–X_2 transitions [2].

The $^5\Sigma^-$ and $^5\Pi$ states which dissociate to the lowest atomic limits (Fig. 1) have $\sigma\pi^4\pi^{*2}\sigma^*$ and $\sigma^2\pi^3\pi^{*2}\sigma^*$ configurations, respectively, and thus have three antibonding orbitals each, hence the repulsive character of their potential curves. The other two $\sigma^2\pi^4\pi^{*2}$ states, a $^1\Delta$ and b $^1\Sigma^+$, have nearly parallel potential curves to that of X $^3\Sigma^-$, but they dissociate to the excited $Sb(^2D_u) + I(^2P_u)$ limit. A similar state of affairs exists for all the group VA halides, and it has the effect of producing somewhat shorter r_e values for the two singlet states than for X $^3\Sigma^-$. The $\pi^* \rightarrow \sigma^*$ $^1\Pi$ does have a shallow potential well, in contrast to its triplet counterpart. This difference in behavior is also easily understandable in terms of their distinct dissociation limits (Fig. 1). The $\sigma \rightarrow \pi^*$ 2 $^3\Pi$ is also slightly bound, but with a notably larger bond length than for 1 $^1\Pi$. The other Λ–S states computed have basically either repulsive potential curves or only rather shallow

minima. The density of states becomes fairly large in the energy region above 25000 cm^{-1}, with eighteen singlet and triplet states converging to the second asymptote, $Sb(^2D_u) + I(^2P_u)$, most but not all of which are indicated in the potential energy diagram of Fig. 1.

3.2. Addition of spin–orbit coupling

When the effects of spin–orbit coupling are included in the molecular Hamiltonian, the series of potential curves shown in Fig. 2 results. The calculated spectroscopic constants of the Ω states are listed in Table 2, along with the corresponding measured results when available. The X $^3\Sigma^-$ Λ–S state is now split in the usual manner for O_2-like molecules, with the $\Omega = 0^+$ multiplet lying lower in energy (Fig. 2). The zero-field splitting gradually decreases to a null value toward large r, however, as both the X_1 0^+ and X_2 1 states correlate with the same atomic limit, $Sb(^4S_{3/2}) + I(^2P_{3/2})$. The X_2 T_e value is computed to be 793 and 753 cm^{-1}, respectively, in the ECP1 and ECP2 treatments (see Section 2 for details of the two calculations). The first of these results is in somewhat better agreement with the corresponding measured zero-field splitting of 965 cm^{-1}, as reported by Winter et al. [1].

There are no experimental bond lengths as yet reported for any of the SbI electronic states, but nearly identical ω_e values of 206 cm^{-1} for X_1 and X_2 have been measured by Winter et al. [1]. An earlier experimental value of 198 cm^{-1} [2] seems to be in error. The full-core ECP2 treatment obtains better agreement with the observed results, but the ECP1 values are only 5–10 cm^{-1} lower. The computed bond lengths for a given state differ by 0.020

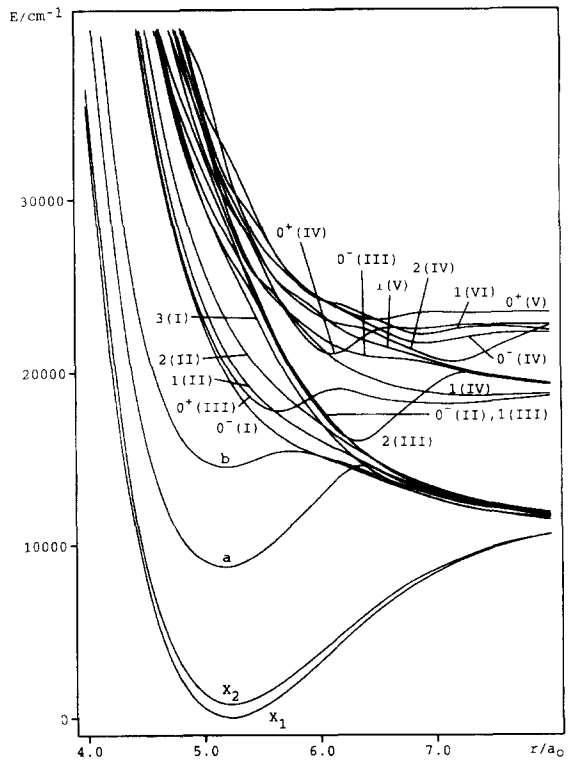

Fig. 2. Potential energy curves of the low-lying Ω states of SbI.

Table 2
Spectroscopic properties of SbI (excitation energy T_e, equilibrium bond length r_e and vibrational frequency ω_e) calculated using semicore (ECP1) and full-core (ECP2) effective core potentials together with corresponding experimental data

State	T_e (cm^{-1})			r_e (Å)		ω_e (cm^{-1})		
	calc.		expt.	calc.		calc.		expt.
	ECP1	ECP2		ECP1	ECP2	ECP1	ECP2	
$X_1\ ^3\Sigma_{0^+}^-$	0	0	0	2.767	2.747	195	201	206 [a]
								198 [b]
$X_2\ ^3\Sigma_1^-$	793	753	965 [a]	2.771	2.751	191	201	206 [a]
a $^1\Delta_2$	8737	8452	(6780) [c]	2.736	2.726	198	196	
b $^1\Sigma_{0^+}^+$	14500	14228	12328 [a]	2.752	2.717	188	189	211 [a]
2(III)	15993			3.351		273		
0^+(III)	17753			2.989		230		
0^+(IV)	21036			3.239		269		

[a] Ref. [1]. [b] Ref. [18].
[c] Estimate given in Ref. [5].

Å in each case. The compositions of the various $\Omega = 0^+$ states in terms of their Λ–S contributions are indicated in Table 3, while the analogous data for the 0^- and 1 states is given in Table 4. There is a moderate amount of b $^1\Sigma^+$ character in $X_1\ 0^+$ (4–6% in the neighborhood of the r_e value), which is critical in the evaluation of the transition moments involving this state, especially for b 0^+–$X_1\ 0^+$ (see Section 3.3). The X_2 1 state by contrast is nearly pure $^3\Sigma^-$ in this region, gradually picking up considerable $^5\Pi$ character for $r \geq 6.0\ a_0$ (Table 4), with the latter change also occurring for $X_1\ 0^+$ (Table 3).

The unobserved a $^1\Delta_2$ state is computed to have a T_e value of 8737 cm^{-1} in the semicore CI treatment and 8452 cm^{-1} in the simpler full-core version. By analyzing the ratios of b 0^+/a 2 T_e values for isovalent systems, Bielefeld et al. [5] have arrived at an estimate of 6780 cm^{-1} for this quantity in SbI, i.e. some 1700–2000 cm^{-1} less than found in the present calculations. Consideration of the different correlation energy errors expected for the $^1\Delta$ and $^3\Sigma^-$ states does indeed suggest that an overestimation in the a 2 T_e value of 1000–2000 cm^{-1} should be expected, so the aforementioned estimate of Ref. [5]

Table 3
Composition of the five lowest 0^+ states of SbI (c^2, %) at various bond distances r (in a_0)

State	r	$1\ ^3\Sigma^-$	$2\ ^3\Sigma^-$	$3\ ^3\Sigma^-$	$1\ ^1\Sigma^+$	$2\ ^1\Sigma^+$	$1\ ^3\Pi$	$2\ ^3\Pi$	$3\ ^3\Pi$	$4\ ^3\Pi$	$1\ ^5\Pi$
$X_1\ ^3\Sigma_{0^+}^-$	4.8	93.0			6.3						
	5.2	93.4			5.4						
	6.0	92.6			4.3						2.0
	8.0	74.5					3.7				19.9
b $^1\Sigma_{0^+}^+$	4.8	6.0			91.9			1.3			
	5.2	5.2			89.8		3.0	1.4			
	5.6	4.2	1.1		62.6		30.8				
	5.8	2.5	1.4		24.7		69.6				
	6.0	1.5	1.5		8.7		84.5				3.0
	6.2	1.2	1.3		3.2		86.9				6.2
	8.0						77.0				21.3
0^+(III)	5.2				3.1		95.8				
	5.4				8.9		89.0				1.1
	5.6				29.9		65.9				2.3
	5.8	1.7			66.4		22.7		1.4		4.6
	6.0	1.5			72.8		5.2	3.0	1.5		14.9
	6.2		1.6		34.5			11.1			51.0
	6.4		2.7		15.1		5.7	13.1			62.0
	6.6	1.1	3.5		9.7		9.9	11.4			63.4
	8.0	19.9					16.2	2.5			56.4
0^+(IV)	5.0		76.9			15.0		6.7			
	5.2		74.3			17.5	1.0	4.4	1.4		
	5.4		42.4			11.1	1.6	6.5	8.2		29.1
	5.6		5.0	1.3		1.4	2.3	20.1	2.4		66.6
	6.0	1.8		1.7	10.0		8.4	17.2	1.1		58.9
	6.2	4.0	1.1	1.4	52.3		10.0	5.9	1.4		22.6
	6.4	5.3	3.1	2.2	68.9	1.0	7.7				10.1
	6.6	7.0		1.1	36.5		4.8	35.6			12.9
	8.0	3.2	3.8	5.4	12.4	1.3		67.8	2.3		
0^+(V)	4.8		8.5		1.1	14.0		75.6			
	5.2		2.1						15.5		80.3
	5.6		64.9			15.9		3.3			12.6
	6.0		48.9			9.2		27.7			8.7
	6.5		20.3	1.8	5.1	1.6		65.7			2.9
	7.0		34.5	21.9	11.7	5.6	2.6	8.9	2.4	5.0	
	8.0		14.5	38.5	17.0				4.5	13.3	
	9.0		5.3	1.3	1.9	1.4			78.9	5.8	

is probably fairly accurate, perhaps some 500 cm^{-1} too low. The calculations indicate that the a 2 r_e value should be 0.02–0.03 Å shorter than that of $X_1\ 0^+$ (Table 2), by virtue of the fact that the $^1\Delta$ dissociates to a higher-lying atomic limit, as discussed in Section 3.1. The present two theoretical treatments agree within 2 cm^{-1} on the value of ω_e for this state, but come thereby to different conclusions as to which of the $X_1\ 0^+$ and a 2 frequencies is the higher. The composition data in Table 5 show that this state is dominated by a $^1\Delta$ up to $r = 6.4\ a_0$, at which point an avoided crossing with the $\Omega = 2$ component of the $\pi^* \rightarrow \sigma^*\ ^3\Pi$ A–S state occurs (Fig. 2). There is also considerable $^5\Pi$ character in the lower state at large r values as well. This avoided crossing produces a potential minimum for the second $\Omega = 2$ state, with a computed r_e value of 3.351 Å (ECP1, Table 2) and a relatively high ω_e value of 273 cm^{-1}.

The b 0^+ state has a complementary composition to that of $X_1\ 0^+$ (Table 3), at least up to $r = 5.5\ a_0$, at which point considerable $^3\Pi$ character is also noted. This latter transformation is again an indication of an avoided crossing, this time with 0^+(III). The b 0^+ potential well is relatively shallow, and for this reason there is somewhat larger disagreement between the two theoretical treatments regarding the r_e value of this state (but not ω_e; Table 2). Consistent with the remarks made previously, it is found that the T_e value of this state is overestimated in both treatments, by from 1900 (ECP2) to 2200 cm^{-1} (ECP1). The experimental T_e value again is taken from the work of Winter et al. [1]. The fact that the computed ω_e values are somewhat lower for b $^1\Sigma_0^+$ than for X $^3\Sigma_{0^+}^-$, while the opposite relationship is observed [1], appears to be closely related to the overestimation of the former's T_e value in the present calculations. If the potential well were 2000 cm^{-1} deeper a larger computed ω_e value would doubtless result (Fig. 2). A total of eight vibrational levels are found in the calculations (ECP1), but in view of the above remarks it seems quite likely that a larger number exists in the experimental spectrum. The intensity distribution of the b–X_1 transition has been analyzed by Winter et al. [1] and we shall return to this point in the next subsection.

The third $\Omega = 0^+$ state starts out at small r as $^3\Pi$ and then gradually takes on more and more b $^1\Sigma^+$

Table 4
Composition of the low-lying 1 and 0^- bound states of SbI (c^2, %) at various bond distances r (in a_0)

State	r	$1\ ^3\Sigma^-$	$2\ ^3\Sigma^-$	$3\ ^3\Sigma^-$	$1\ ^3\Pi$	$2\ ^3\Pi$	$3\ ^3\Pi$	$1\ ^1\Pi$	$1\ ^3\Delta$	$1\ ^3\Sigma^+$	$1\ ^5\Sigma^-$	$1\ ^5\Pi$
$X_2\ ^3\Sigma_1^-$	4.8	99.1										
	5.2	98.6										
	5.7	97.5										1.3
	6.0	96.4										2.5
	8.0	72.9			3.7							21.2
1(VI)	4.8		30.6					18.8 [a]	30.4	10.4	1.4	
	5.2		40.6							45.1	5.4	4.3
	6.0		7.7	1.8	9.0	5.3	1.9	52.4		1.8	8.1	7.8
	6.8				3.6	50.1		19.1	15.4			4.7
	7.5		13.1	1.1		42.3	1.2	20.2	11.0			
	8.0		6.4	2.2		57.8		9.2	13.1			

State	r	$1\ ^3\Pi$	$2\ ^3\Pi$	$3\ ^3\Pi$	$4\ ^3\Pi$	$1\ ^5\Sigma^-$	$1\ ^5\Pi$	$1\ ^3\Sigma^+$	$2\ ^3\Sigma^+$	$1\ ^1\Sigma^-$	$2\ ^1\Sigma^-$
0^-(IV)	4.8		10.4			60.3	23.7	3.2			
	5.2		49.8	2.9			7.2	28.3		11.1	
	6.0		5.5			12.9	19.3	29.0		31.3	
	6.5	5.2	21.3			18.4	34.0	4.4		13.2	
	6.8	3.5	54.4				20.5	7.0		9.5	
	7.5		71.2		2.2				4.6	16.5	
	8.0		77.6					4.1	3.0	1.1	7.1
	9.0			59.4	19.7			3.5	7.3		3.0

[a] Contribution of the $2\ ^1\Pi$ state.

and $^5\Pi$ character (Table 3). It has an r_e value of 2.989 Å according to the ECP1 calculations and a relatively high ω_e value by virtue of the avoided crossing with the lower 0^+ state (Table 2, Fig. 2). Bound–bound transitions to $X_1\ 0^+$ and $X_1\ 1$ may be observable as a result, unless heterogeneous predissociation by the second $\Omega = 1$ state dominates over such a radiative process. Another avoided crossing occurs between the third and fourth $\Omega = 0^+$ states (Fig. 2) at fairly large r where the $^5\Pi$ Λ–S state begins to dominate in the lower of these two states. Still another avoided crossing is found between 0^+(IV) and 0^+(V). The second through the fifth $\Omega = 1$ states are found to be repulsive, whereas 1(VI) shows a weak potential minimum around $r =$ 7.0 Å. This state has a fairly complex composition in terms of a number of Λ–S states (Table 4), as one would expect in view of the relatively high density of states in this energy region.

The lowest atomic limit, $Sb(^4S_{3/2}) + I(^2P_{3/2})$ correlates with ten molecular states: $\Omega = 0^+(2)$, $0^-(2)$, 1(3), 2(2) and 3(1). As a result, the a 2 and b 0^+ states go to the same limit as the $X_1\ 0^+$ and $X_2\ 1$ species, despite the fact that the $^1\Sigma^+$ and $^1\Delta$ Λ–S states have a higher-lying asymptote than $X\ ^3\Sigma^-$ (see Fig. 1 and the discussion in Section 3.1). It is also interesting that the $^3\Pi_{0^-}$ state is repulsive, while its $\Omega = 0^+$ counterpart is bound by virtue of the avoided crossing already discussed.

At $r = 9.0\ a_0$ the merging of all ten potential curves which go to the $Sb(^4S_{3/2}) + I(^2P_{3/2})$ limit is quite evident, with a maximum spread in the corresponding computed energy values of 548 cm^{-1}. This result is a good indication that the AO basis limit has

Table 5
Composition of the four lowest $\Omega = 2$ states of SbI (c^2, %) at various bond distances r (in a_0)

State	r	$1\ ^3\Pi$	$2\ ^3\Pi$	$3\ ^3\Pi$	$4\ ^3\Pi$	$1\ ^1\Delta$	$2\ ^1\Delta$	$1\ ^3\Delta$	$2\ ^3\Delta$	$1\ ^5\Sigma^-$	$1\ ^5\Pi$
$a\ ^1\Delta_2$	4.8					98.8					
	5.2	1.0				98.4					
	5.7	1.3				96.9					
	6.0	3.4				93.6					
	6.5	40.7				5.8				5.7	46.1
	7.0	28.3									70.3
	9.0	46.1								14.3	38.8
2(II)	4.8	94.4								4.4	
	5.2	90.2								7.7	
	6.0	60.4				4.2				19.7	13.0
	6.3	1.7				9.5				9.0	78.1
	7.0	24.2								60.7	14.3
	9.0	4.3								51.4	44.2
2(III)	4.8		73.2					22.7		1.5	
	5.0		52.0					37.2		5.1	3.8
	5.2		20.1					27.2		15.6	36.0
	5.4		2.4	1.8				6.7		17.0	71.8
	5.8			1.0				1.7		18.2	78.6
	6.0		1.2					1.1		24.7	71.8
	6.2	11.5				2.7				41.5	43.2
	6.4	12.3				67.9				16.2	1.0
	6.6					90.7				3.5	1.0
	7.0	1.6			6.9	84.4				4.0	
	9.0	47.0								34.1	16.8
2(IV)	4.8		17.9				10.8	67.4			3.0
	5.2		29.8	3.5			2.4	13.1			49.7
	6.0	27.9	22.7	5.8			1.6	2.6		31.3	7.2
	6.5	42.1	2.1			1.2				41.1	11.4
	7.0	43.1				6.2				34.4	13.1
	7.5	2.2	2.0		13.1	79.8					
	9.0		12.6	23.3		45.4	6.9	1.9	5.5		

been closely approached in the present CI treatment, since one knows that at infinite separation all such energy values become exactly equal in a full CI. Based on these findings an average D_e value for the X_1 0^+ state of 11344 cm^{-1} or 1.407 eV is predicted. Since this system is isovalent with O_2, for which the corresponding ground state D_e value can be obtained to an accuracy of ± 0.2 eV with a relatively simple CI treatment [19], there is good reason to believe that the present SbI result should be close to the experimental value, but no such result is yet available to confirm this point. Compositions of the various $\Omega = 0^+$, 0^-, 1 and 2 states in this group may be taken from Tables 3–5. The $\Omega = 3$ species comes mainly from the lowest $^5\Pi$ state.

The $Sb(^4S_{3/2}) + I(^2P_{1/2})$ atomic limit is next in order and correlates with five molecular states: $\Omega = 0^+$, 0^-, 1(2) and 2. All these states converge nicely to this asymptote as well (Fig. 2), with energy results at $r = 9.0$ a_0 ranging from 18800 to 19000 cm^{-1}. The average of these values is 18911 cm^{-1}. This corresponds to an iodine atom ^2P_u zero-field splitting of 7567 cm^{-1}, which is in very good agreement with the observed energy separation of 7609 cm^{-1} [20]. The 0^+(III) and 2(III) are bound states which go to this limit (Fig. 2). There is an avoided crossing involving the lowest three states of $\Omega = 2$ symmetry near the r_e value of 2(III). The results of Table 5 show that the latter state changes its dominant Λ-S character from $^3\Pi$ at small r to $^5\Pi$ near $r = 5.3$ a_0 and finally to $^1\Delta$ beyond $r = 6.3$ a_0.

The next atomic limit is $Sb(^2D_{5/2}) + I(^2P_{3/2})$. The antimony ^2D–^4S excitation energy is overestimated by 2000–3000 cm^{-1} on the basis of the present large-r computations. This result is to be expected because the correlation energy error for the ^2D state is notably larger than for the ^4S Λ–S state of the same atomic configuration but higher multiplicity. There are 24 states of various Ω symmetries (14 for $J = 5/2$ and 10 for $J = 3/2$) which correlate with the two $Sb(^2D) + I(^2P_{3/2})$ atomic limits, most but not all of which are also indicated in Fig. 2. Since the Sb ^2D zero-field splitting is relatively small (1342 cm^{-1}) and there is the usual spread among the corresponding long-distance molecular energy results, it is rather difficult to distinguish between these two asymptotic values in the figure, however.

Table 6
Calculated lifetimes of excited states of SbI ($v' = 0$): partial lifetimes τ_0 and τ_1 for transitions to X_1 $^3\Sigma_{0^+}^-$ and X_2 $^3\Sigma_1^-$, respectively, and total lifetime τ obtained with ECP1

State	τ_0 (s)	τ_1 (s)	τ (s)
X_2 $^3\Sigma_1^-$	36.9		36.9
a $^1\Delta_2$		9.2×10^{-3}	9.2×10^{-3}
b $^1\Sigma_{0^+}^+$	17.3×10^{-6}	154×10^{-6}	15.6×10^{-6}
	26.5×10^{-6}	428×10^{-6}	25.0×10^{-6} [a]
2(III)		1.6×10^{-3}	1.6×10^{-3}
0^+(III)	92×10^{-6}	54×10^{-6}	34×10^{-6}
0^+(IV)	3.9×10^{-6}	500×10^{-6}	3.9×10^{-6}

[a] Calculated with ECP2.

3.3. Intensity and dipole moment results

The relative intensities of the SbI b–X_1 and b–X_2 transitions have also been studied experimentally by Winter et al. [1]. To consider this aspect of the SbI spectrum we have computed the electric dipole transition moments of different pairs of vibrational states for various bound–bound processes. The results of these calculations are given in Table 6 in the form of radiative lifetimes of the $v = 0$ levels of various excited electronic states. The X_2 $^3\Sigma_1^-$ state is found to have a long lifetime of 36.9 s. This result can be anticipated from the composition data for the X_1 and X_2 states in Tables 3 and 4 since the upper state is almost pure $^3\Sigma^-$ in the Franck–Condon region and X_1 has almost no contribution from $^3\Pi$ states. In addition, the relatively low energy of the X_2–X_1 transition tends to minimize the value of its Einstein coefficient.

The a $^1\Delta_2$ state has not yet been located experimentally and the computed lifetime of 0.01 s (Table 6) shows that it is difficult to observe transitions from it to lower states. The results of Table 5 indicate that there is only a small admixture of $^3\Pi$ character in the a $^1\Delta_2$ wavefunction in the FC region, and the a–X_2 Ω-allowed transition is also weak because of the low energy involved. It seems more likely that this state can be detected on the basis of emissions to it from higher-lying states, but the present results do not indicate any obvious bound state of $\Omega = 1$ symmetry for this purpose (Fig. 2). In addition neither the weakly bound 2(III) or 2(IV) states seem very promising in this respect.

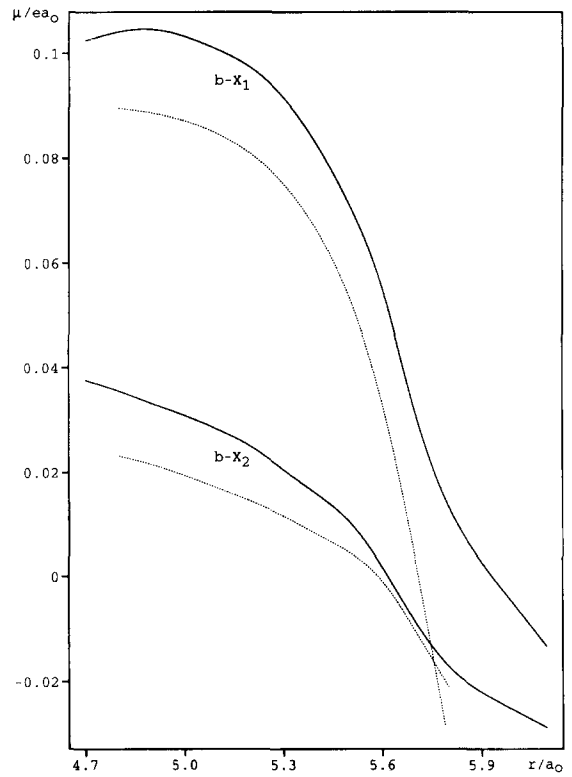

Fig. 3. Comparison of the calculated dipole transition moments for the b–X_1 and b–X_2 processes in two different theoretical treatments (ECP1: solid lines, ECP2: dotted lines).

The transition moments for the b–X_1 (μ_z) and b–X_2 (μ_x) processes computed in the two theoretical treatments of the present study are given as a function of internuclear distance in Fig. 3. There is good agreement between the two sets of calculations, especially with respect to the shapes of the two curves. The ECP1 treatment, with the semicore RECP [10] and the more extensive CI, gives slightly more positive results at each r value considered for both processes. Both transition moments decrease with r, the b–X_1 quantity more sharply. It is clear that in the FC region the b–X_2 transition moment is the much smaller of the two, and this is in qualitative agreement with Colin's rules [2].

Experimentally it has not been possible to completely resolve the vibrational structure in these two band systems [1]. Because the potential curves of all three of the participating states are so nearly parallel (Fig. 2), the various b–X $\Delta v = 0$ transitions have very similar wavelengths and so this result is easily understandable from a theoretical point of view. It was possible to compare the intensities of the b–X_1 and b–X_2 band systems for their respective $\Delta v = 0$ sequences, however, and Winter et al. [1] have reported that their ratio is 0.013, with that of b–X_1 by far the stronger of the two. It is unclear how to compute this result theoretically since some sort of averaging over a number of transitions in both band systems is involved. It is found that the ratios for individual $\Delta v = 0$ vibrational transitions decrease rather quickly with v. A simple arithmetic average of the calculated first eight $\Delta v = 0$ Einstein coefficients leads to ratios of 0.0806 and 0.0470 for the ECP1 and ECP2 treatments, respectively. Although the agreement with the corresponding experimental result is by no means quantitative, it certainly is qualitatively consistent with the overriding conclusion of Winter et al.'s work, namely that the b–X_1 0^+ transition is much stronger than its b $\rightarrow X_2$ 1 counterpart. It should also be noted, however, that the strong variations in the pertinent transition moments with internuclear distance, especially since the b–X_2 value passes through zero (Fig. 3), make it imperative to know the actual populations of the various upper vibrational levels in order to obtain a meaningful theoretical comparison for this ratio.

Table 7
Electric dipole moment values μ (in ea_0) of the $X_1\ ^3\Sigma_{0^+}^-$ and b $^1\Sigma_{0^+}^+$ states as a function of internuclear distance, all values correspond to $Sb^+ I^-$ polarity

r (a_0)	$X_1\ ^3\Sigma_{0^+}^-$	b $^1\Sigma_{0^+}^+$
4.8	−0.384	−0.081
4.9	−0.481	−0.157
5.0	−0.575	−0.239
5.1	−0.666	−0.315
5.2	−0.755	−0.391
5.25	−0.797	−0.425
5.3	−0.836	−0.459
5.4	−0.909	−0.523
5.5	−0.972	−0.573
5.6	−1.030	−0.614
5.7	−1.079	−0.633
5.8	−1.123	−0.617
5.9	−1.160	−0.566
6.0	−1.193	−0.479

It is quite interesting that the opposite relationship has been found both in experiments [2] and calculations for SbF [3] and other group VA fluorides [6]. Analysis of the present computed results shows that the cause for this distinction is closely tied up with the magnitude of the electronegativity difference of the constituent atoms in the various molecules. To see this it is important to know that in all molecules of this type the $b \rightarrow X_1$ transition moment is roughly proportional to the difference in the electric dipole moments of the upper and lower states. As pointed out earlier [3], in fluorides both dipole moments are relatively large but nearly equal to one another, whereas for the heavier halogen-containing systems such as SbI this difference in dipole moments is significantly larger because the overall degree of polarity is smaller and much more dependent on the nature of the electronic state of the system. The present computed electric dipole moments are given in Table 7 for a number of internuclear distances, from which it is seen that $\mu(X_1)$ and $\mu(b)$ typically differ by 0.3–0.4 ea_0 in the SbI Franck–Condon region. By contrast, the analogous differences in SbF fall only in the 0.05 ea_0 range [3]. The $b–X_2$ 1 transition moments are not strongly influenced by such charge polarity effects, and so as a result the $b–X_1$ value can be larger or smaller in absolute magnitude in such systems depending on how greatly the electronegativities of the constituent atoms differ, consistent with Colin's original observations [2]. At the same time it is well to note that the BiF molecule represents an exception to this rule, but this is because the strength of the spin–orbit coupling in this heavy-atom system produces a more complicated picture. Two low-lying $\Omega = 0^+$ states exist in this case, with varying amounts of both $^1\Sigma^+$ and $^3\Pi$ character, as discussed in earlier work [4].

Another measure of the relative strengths of the two b–X transitions is based on the magnitude of the partial lifetimes of the upper state in the respective processes (defined as the reciprocal of the sum of the Einstein coefficients for all vibrational transitions into a given lower electronic state). The present computed values in both the ECP1 and ECP2 treatments for these quantities are given in Table 6, from which it is seen that the $b–X_1$ result is an order of magnitude shorter than that of $b–X_2$. A somewhat larger ratio is found in the ECP2 treatment. The radiative lifetime of the b state is thus calculated to be 15.6 μs in the ECP1 treatment and 25.0 μs in ECP2. There is thus again a good level of agreement between the two theoretical treatments in this case, but unfortunately there is no experimental value for the lifetime of any of the SbI excited states. In both cases the $b–X_2$ emissions are almost negligible in obtaining these results. In SbF the opposite order of partial lifetimes has been computed [3], 2230 μs for $b–X_1$ and 58.5 μs for $b–X_2$, in agreement with Colin's rules [2]. The computed value for the SbF total lifetime [3] is 57.0 μs, several times longer than that in SbI. Radiative lifetimes for the lighter antimony halides (F, Cl, Br) have been estimated from measurements [5] to lie in the 150–450 μs range, with an indication that the value becomes longer with increasing atomic number.

Three other lifetimes are listed in Table 6, of which that for 2(III) is the longest (1.6 ms). The 0^+(IV) state is computed to have the shortest lifetime of any of the low-lying SbI states (3.9 μs). Reference to Fig. 2 shows that the low-v' transitions from this state to either X_1 or X_2 go into very high v'' levels. Parallel transitions to X_1 0^+ are highly favored over their perpendicular counterparts to either X_1 or X_2, reflecting the fact that 0^+(IV) is dominated by the $2\ ^3\Sigma^-$ A-S state in the Franck–Condon region. It is also found that 0^+(IV)–b 0^+ transitions are relatively strong, with a partial lifetime of 10 μs having been computed. The lifetime of the third 0^+ state is about twice as long as for the b state.

4. Conclusion

Two spin–orbit CI theoretical treatments have been employed to study the electronic structure and spectrum of the SbI molecule. Even without correlation of the Sb 4d electrons, it has been possible to obtain quite accurate ω_e values in these calculations. The ground state $X\ ^3\Sigma^-$ zero-field splitting is underestimated by about 200 cm^{-1} or roughly 20%. The T_e value of the well-studied b state is overestimated by 1900 and 2200 cm^{-1} in the two treatments. This result is expected from standard correlation energy arguments. On this basis the T_e value of the as yet unobserved a $^1\Delta_2$ state is placed near 7000

cm^{-1}, which is in good agreement with the estimate of Bielefeld et al. [5] based on a comparison of observed b/a T_e ratios in other diatomics with 12 valence electrons.

The computed intensity of the b–X_1 transition is found to be much larger than for b–X_2, in agreement with the observations of Winter et al. [1]. The opposite relationship has been obtained earlier for SbF [3], as found empirically by Colin et al. [2]. An explanation for this result has been given in terms of the electronegativity differences of the constituent atoms. The computed radiative lifetime for the b 0^+ state is 16.4 μs in the ECP1 treatment and 25.7 μs in ECP2. Several other bound states of $\Omega = 0^+$ and 2 symmetry have also been identified in the calculations in the 16000–21000 cm^{-1} range.

The dissociative behavior of the various potential energy curves has also been carefully studied. Computed energies at large r values for molecular states which correlate with the same atomic limit are found to agree within a few hundred cm^{-1}, indicating that the full CI limit has been closely approached in both the present theoretical treatments. The X_1 0^+ D_e value is predicted to be 1.41 eV on this basis, but there is no measured value with which to compare. The computed iodine atom ^2P_u zero-field splitting (7567 cm^{-1}) is found to be in quite good agreement with experiment (7603 cm^{-1}), however, based on a comparison of long-distance molecular state energy results at large internuclear separations.

Acknowledgement

The authors wish to thank Professor R.M. Pitzer for making available his ECP spin–orbit integral program to them. One of us (KKD) would like to thank the Commission of the European Communities and the Government of India for providing the Marie-Curie fellowship. One of us (ABA) thanks the Alexander von Humboldt foundation for the granting of a stipend. This work was supported in part by the Deutsche Forschungsgemeinschaft in the form of a Forschergruppe grant and within the Schwerpunktprogramm 'Theorie relativistischer Effekte in der Chemie und Physik schwerer Elemente'. The financial support of the Fonds der Chemischen Industrie is also hereby gratefully acknowledged.

References

[1] R. Winter, H. Kruse, E.H. Fink, J. Wildt and F. Zabel, Chem. Phys. Letters 104 (1984) 383.
[2] R. Colin, M. Herman and F. Prevot, Chem. Phys. Letters 91 (1982) 213.
[3] I. Boustani, S.N. Rai, H.-P. Liebermann, A.B. Alekseyev, G. Hirsch and R.J. Buenker, Chem. Phys. 177 (1993) 45.
[4] A.B. Alekseyev, H.-P. Liebermann, I. Boustani, G. Hirsch and R.J. Buenker, Chem. Phys. 173 (1993) 333.
[5] M. Bielefeld, G. Elfers, E.H. Fink, H. Kruse, J. Wildt, R. Winter and F. Zabel, J. Photochem. 25 (1984) 419.
[6] H.-P. Liebermann, I. Boustani, S.N. Rai, A.B. Alekseyev, G. Hirsch and R.J. Buenker, Chem. Phys. Letters 214 (1993) 381.
[7] A.B. Alekseyev, H.-P. Liebermann, R.J. Buenker and G. Hirsch, J. Chem. Phys. 102 (1995) 2539.
[8] A.B. Alekseyev, H.-P. Liebermann, R.J. Buenker, G. Hirsch and Y. Li, J. Chem. Phys. 100 (1994) 8956.
[9] K. Balasubramanian, Chem. Phys. Letters 127 (1986) 324.
[10] L.A. LaJohn, P.A. Christiansen, R.B. Ross, T. Atashroo and W.C. Ermler, J. Chem. Phys. 87 (1987) 2812.
[11] R.J. Buenker and S.D. Peyerimhoff, Theoret. Chim. Acta 35 (1974) 33; 39 (1975) 217;
R.J. Buenker, S.D. Peyerimhoff and W. Butscher, Mol. Phys. 35 (1978) 771.
[12] R.J. Buenker and R.A. Philips, J. Mol. Struct. THEOCHEM. 123 (1985) 291.
[13] E.R. Davidson, in: The world of quantum chemistry, eds. R. Daudel and B. Pullman (Reidel, Dordrecht, 1974) p. 17.
[14] G. Hirsch, P.J. Bruna, S.D. Peyerimhoff and R.J. Buenker, Chem. Phys. Letters 52 (1977) 442.
[15] D.B. Knowles, J.R. Alvarez-Collado, G. Hirsch and R.J. Buenker, J. Chem. Phys. 92 (1990) 585.
[16] J.W. Cooley, Math. Comput. 15 (1961) 363.
[17] M. Perić, R. Runau, J. Römelt, S.D. Peyerimhoff and R.J. Buenker, J. Mol. Spectry. 78 (1979) 309.
[18] N. Danon, A. Chatalic, P. Deschamps and G. Pannetier, C.R. Acad. Sci. Paris C 269 (1969) 1249.
[19] S.D. Peyerimhoff and R.J. Buenker, Chem. Phys. Letters 16 (1972) 235.
[20] C.E. Moore, Arch. US Natl. Bur. Stand. No. 467, Vol. 1 (1971).